



A 3D-printed coaxial microfluidic device approach for generating magnetic liquid metal droplets with large size controllability

Xiaokang He¹ · Jie Wu¹ · Tao Hu¹ · Shouhu Xuan^{1,2} · Xinglong Gong¹

Received: 4 December 2019 / Accepted: 21 March 2020 / Published online: 3 April 2020
© Springer-Verlag GmbH Germany, part of Springer Nature 2020

Abstract

The monodisperse magnetic liquid metal droplets have been proven to be very important in soft robots or machines and flexible electronics. Unfortunately, the size and composition tunability is technically confined due to the scarce of the preparation method. This paper reports a 3D-printed coaxial microfluidic device to generate monodisperse magnetic liquid metal droplets (MLMDs) with droplets sizes varied in a large range of 650 to 1900 μm . Owing to the inner-dispersed iron/nickel (Fe/Ni) particles, the MLMDs with different magnetic contents possess unique magnetic field manipulation performance. The minimum magnetic flux density driven the MLMDs is only 24 mT and the relative average actuating velocity reaches as high as 5.1 cm/s, which means that the MLMDs can be precisely and rapidly manipulated. In addition, the manipulation of the MLMDs by an external magnetic field has been illustrated in two-dimensional crooked channels and three-dimensional spiral channels. The MLMDs move through the two kinds of channels smoothly and exhibit good magnetic maneuverability. Finally, the potential feasibility of the MLMDs is further confirmed in small-sized electrical switches with the sequential turning on of light-emitting diodes (LEDs).

Keywords Magnetic liquid metal droplets · Size controllable · 3D-printed device · Microfluidic · Magnetic manipulation

1 Introduction

Recently, gallium-based room temperature liquid metal alloys such as Galinstan or EGaIn have been widely used due to their high surface tension, good flexibility, high electrical/thermal conductivity, and low toxicity (Dickey 2014; Liu et al. 2012). These liquid metals show a wide

variety of potential applications, including microelectromechanical (MEMS) actuators (Bartlett et al. 2017; Shu et al. 2018; Tang et al. 2014), flexible and wearable electronics (Chu et al. 2018; Hu et al. 2018; Ilyas et al. 2017), robotics (Wang et al. 2019; Wu et al. 2018), and microfluidics (Khoshmanesh et al. 2017). Among them, the magnetic manipulation of liquid metals is of great significance. Most commonly, the manipulation of liquid metals by an external magnetic field is achieved via the modification of their surface with magnetic particles. For example, liquid metal droplets coated with iron (Fe) particles can be obtained in microfluidic channels and applied on electrical switches using an external magnetic field (Bilodeau et al. 2017; Jeon et al. 2016, 2017; Jeong et al. 2019).

Versatile magnetic liquid metal droplets (MLMDs) have been developed by altering the synthesizing method. Other metal particles such as Cu also can be mixed with Fe and uniformly dispersed in the liquid metal droplets. These liquid metal droplets can be controlled using both magnetic and electric fields (Li et al. 2019). Further research has shown that nickel (Ni) can be electroplated on the surface of liquid metal and the as-formed magnetic liquid metal droplet (MLMD) motor can achieve autonomous locomotion by

Electronic supplementary material The online version of this article (<https://doi.org/10.1007/s10404-020-02336-4>) contains supplementary material, which is available to authorized users.

✉ Shouhu Xuan
xuansh@ustc.edu.cn

✉ Xinglong Gong
gongxl@ustc.edu.cn

¹ CAS Key Laboratory of Mechanical Behavior and Design of Materials, Department of Modern Mechanics, CAS Center for Excellence in Complex System Mechanics, University of Science and Technology of China, Hefei 230027, People's Republic of China

² National Synchrotron Radiation Laboratory, University of Science and Technology of China, Hefei 230027, People's Republic of China

reacting with aluminum foil (Zhang et al. 2016). Although these aforementioned liquid metal droplets showed promising mobility and exhibited extraordinary properties, the size of these droplets was not controllable, which critically limited their application in the micro-scale field. Therefore, an easy method capable of generating size controllable MLMDs is pressing needed.

With the development of microfluidic techniques, droplet-based microfluidics is becoming a highly useful platform for generating micro-droplets (Lee et al. 2009, 2016b; Nguyen et al. 2018). Various liquid metal droplets with different diameters have been generated based on the microfluidic chips (Hutter et al. 2012; Jin et al. 2019; Tang et al. 2016). The well-known fabrication method for microfluidic chips is soft lithography. This method requires complicated manual operations and is quite time-consuming, which brings difficulties for applying the microfluidic techniques in generating liquid metal droplets. In addition, platforms that produce liquid metal droplets with smaller particle sizes need more precise control and higher equipment requirements. It is only suitable for professionals and is not easy to promote. In recent years, with the advantages of high precision and easy usage, 3D-printed technology gets through a rapid development in additive manufacturing (Bhattacharjee et al. 2016; Lee et al. 2016a; Yazdi et al. 2016). Based on the simple and low-cost 3D-printed fabrication process, various microfluidic devices are increasingly used to get different kinds of droplets (Ji et al. 2018; Song et al. 2019; Zhou et al. 2018). These devices can be used in a plug-and-play manner and are capable of controlling the size and shape of the droplets. To this end, applying the 3D-printed microfluidic devices to generate size controllable MLMDs become a potential solution.

In this work, a 3D-printed coaxial microfluidic device was developed to generate monodisperse magnetic liquid metal droplets (MLMDs) with a large size variation range. The magnetic liquid metal was obtained as dispersed phase by dispersing Fe/Ni particles inside the liquid metal. The relationship between the diameter of MLMDs and the flow rate ratio of the two phases was studied. Subsequently, the minimum magnetic flux density and the average actuating velocity required to drive the MLMDs with different Fe/Ni particle contents were controlled in this method. In addition, the manipulation of the MLMDs in crooked channels with different angles and three-dimensional spiral channels demonstrated that the MLMDs could be manipulated by the magnetic field very well. Finally, by turning on/off of the LED lamps, the MLMDs showed a wonderful electrical switching applicability in the microfluidic channels.

2 Materials and method

2.1 Device fabrication

The coaxial microfluidic device used in the experiments was designed by SolidWorks 2013 (Dassault Systemes S.A, Inc., USA) and then printed on the ProJet 3500 HDMax (3D Systems, Inc., USA). The highest resolution of the printer is $750 \times 750 \times 1600$ DPI, which means that the minimum line width in xy plane is $34 \mu\text{m}$ and the minimum layer thickness is $16 \mu\text{m}$. The minimum orifice of the coaxial microfluidic device is $250 \mu\text{m}$, which means the resolution is sufficient for the accuracy of the devices. There were two kinds of materials (photosensitive resin and wax) used for printing the devices. The wax was used as a kind of sacrificed material for this device, and it can be easily removed by heating it in a water bath.

The fabricated coaxial microfluidic device (Fig. 1d) consisted of three modules, a top module (Fig. 1a), an intermediate module (Fig. 1b) and a bottom module (Fig. 1c). The cross-sectional illustrations of the designed three modules and the coaxial microfluidic device were shown in Fig. S2. Different modules were connected to each other by triangular threads to ensure a reliable sealing property (Morimoto et al. 2018). The top module has a hollow cylinder and an inlet for the passage of the dispersed phase. The intermediate module has two coaxial hollow cylinders and an inlet for the passage of the continuous phase. The bottom module has an orifice to form monodisperse droplets under the coaxial flow-focusing mechanism and an outlet port to release the droplets, and the orifice diameter can be changed to vary the droplets diameter. The intermediate module also has an orifice for the infusion of the dispersed phase, and it can connect with other microfluidic modules at both its inlet and outlet using screw threads.

As we know, the coaxial flow focusing mechanism is to form droplets by overcoming the surface tension of the continuous phase by the shear stress of the dispersed phase (Gu et al. 2011). Figure 1e shows the general structure of the axisymmetric channel in coaxial microfluidic device and the process for producing MLMDs. The formation type of droplets depends on the capillary number Ca of the interface between the inner and outer fluid. When $Ca < 1$, the droplets are formed in the dripping mode and their monodispersity is better than those formed in the jetting mode ($Ca > 1$). Figure 1f shows the typical preparation of MLMDs in the dripping mode, the droplets are formed close to the exit of the orifice. In this mode, dispersed phase occupies a fraction of space of the throat, continuous phase can flow through the orifice easily, and thus viscous force F_μ (caused by the viscous stress acting on the

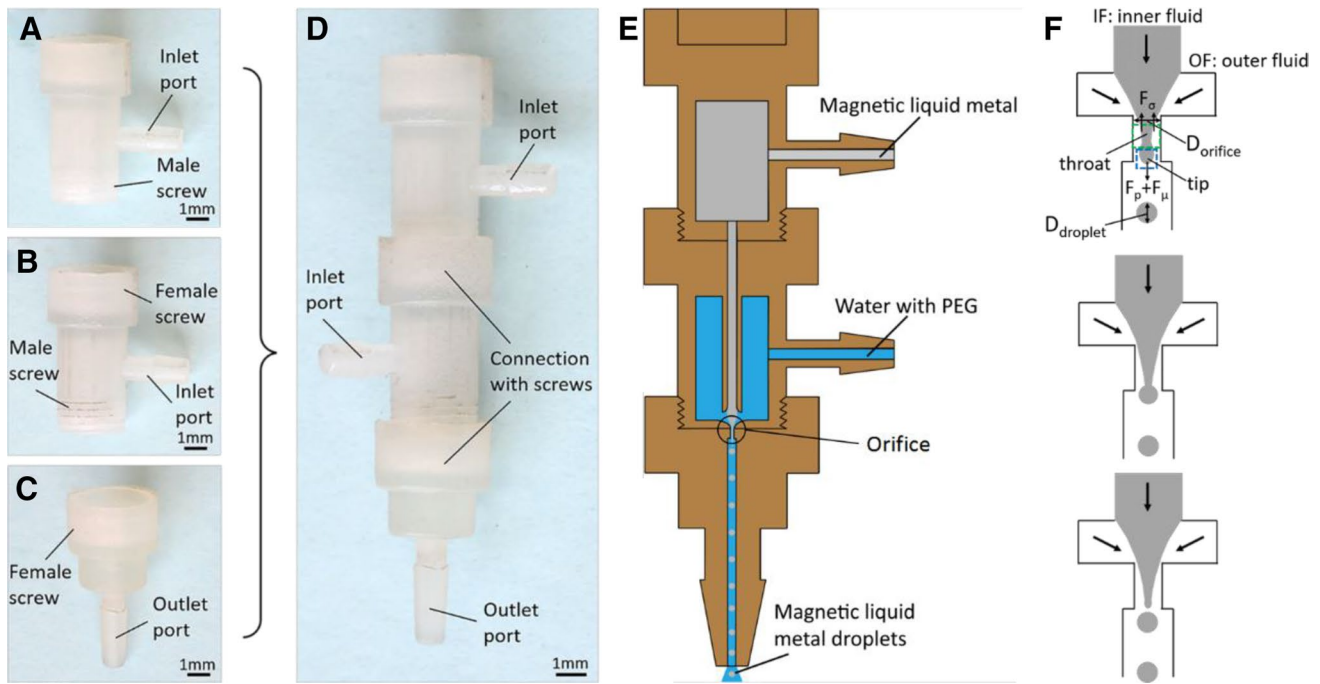


Fig. 1 Images of coaxial microfluidic devices. **a** Image of top module, **b** intermediate module, **c** bottom module and **d** coaxial microfluidic device composed of three modules. **e** Schematic formation pro-

cess for producing MLMDs. **f** Formation sequence of MLMDs in the dripping regime

interface) combining with the interfacial tension force F_σ determines the breakup of droplet. The hydrostatic pressure F_p is not the key parameter of breakup in this mode. With the pump of dispersed phase, tip starts to grow, and F_μ stretches the tip moving downstream until the weaker F_σ is no longer strong enough to hold the tip. To this end, the droplet is formed. The droplet diameter can be predicted by the following equation,

$$D_{\text{droplet}} = C \frac{D_{\text{orifice}}}{\sqrt{\frac{Q_{\text{OF}}}{Q_{\text{IF}}} + 1}} \tag{1}$$

where D_{droplet} is the diameter of the generated droplets, D_{orifice} is the diameter of the orifice in the bottom module, Q_{OF} and Q_{IF} are the flow rate of the outer and inner fluid, C is a constant value depending on the properties of the fluids used. From this formula, the size of droplets was controllable by changing the flow rate ratio (Morimoto et al. 2009).

2.2 Preparation of magnetic liquid metal

In order to form monodisperse MLMDs with controllable sizes, water containing 15 wt% poly(ethylene glycol)(PEG) was used as the continuous phase, and magnetic liquid metal (Galinstan) was used as the dispersed phase. The magnetic

liquid metal was obtained by mixing magnetic particles into Galinstan liquid metal with 1 mol/L HCl solution. To increase the content of magnetic particles in the obtained MLMDs, the liquid metal was, respectively, mixed with three kinds of magnetic particles: iron (Fe) particles (6 μm), nickel (Ni) particles (5 μm) and Fe/Ni particles (mass ratio 1:1) (Fig. S1). Firstly, 80 μL of liquid metal and 50 mg magnetic particles were mixed. Then an appropriate amount of HCl solution was added and the mixture was stirred for 15 min until the absorption of the magnetic particles by the liquid metal was saturated. During the mixing process, the mass variation of liquid metal was measured to calculate the absorption rate. The calculation results in Table S1 of the Supporting Information indicated that Fe/Ni particles have the highest absorption rate than the other two kinds of particles. Therefore, the method of mixing liquid metal with Fe/Ni particles was chosen in this paper. Since the increase in the Ni content reduced the fluidity of the Galinstan liquid metal, the maximum Fe/Ni content in magnetic liquid metal was controlled at 10 wt% (Ma et al. 2019).

2.3 Materials and experimental setup

The galinstan liquid metal, iron (Fe) and nickel (Ni) particles were purchased from Sigma-Aldrich. Poly(ethylene glycol) (PEG), Hydrochloric acid(HCl) and Tween 20 were obtained from Sinopharm Chemical Reagent Co., Ltd. Deionized

water was used in these experiments. The micromorphology of the MLMDs was observed by means of scanning electron microscopy (SEM) and related energy-dispersive X-ray spectrum (EDX) (SEM 500, Zeiss, Ltd.). A magnetic property measuring system (MPMS) vibrating sample magnetometer (VSM) (SQUID, Quantum Design Co., America) was used to study the magnetic hysteresis loops of the MLMDs with different Fe/Ni particle contents. The rheological properties of the magnetic liquid metal were carried out by a commercial rheometer (Physica, MCR 302, Anton Paar Co., Austria) with a magnetic field generator. The images of the MLMDs were captured via the microscopy and a CCD camera (Nikon, Japan). Acrylonitrile butadiene styrene (ABS) materials were used to print the models in Fig. 8 and 9 and the printing temperature of this material was 220 °C.

3 Results and discussion

3.1 Generation of the MLMDs

The preparation process of the magnetic liquid metal was shown in Fig. 2a. 0.37 g Fe/Ni particles were added into 0.5 mL Galinstan liquid metal, then 1 mol/L HCl solution was added and stirred at room temperature for 15 min. Finally, the magnetic liquid metal with Fe/Ni content of 10 wt% was obtained. Before the addition of the HCl solution, there was an oxide layer on the surface of the liquid metal due to exposure to the air. This oxide layer hinders the absorption of Fe/Ni particles into the liquid metal and makes it appear non-spherical. The HCl solution removes the oxide layer on the surface of the liquid metal, and the Fe/Ni particles can be well mixed with the liquid metal (Hu et al. 2019). After adding the HCl solution, the liquid metal turned to have a curve surface due to the changed surface tension. Figure 2b displays the SEM images of the liquid metal before and after stirring with HCl solution. Clearly, its surface changed from smooth to rough after stirring, which must be attributed to the addition of magnetic particles. Originated from the magnetic Fe/Ni contents, the magnetic liquid metal had the characteristic magnetic property and the hysteresis loops of the samples were investigated by a MPMS VSM at room temperature (Fig. 2c). All the hysteresis loops were smooth and no hysteresis was found, which indicated the coercive forces and the residual magnetizations approached to zero. Clearly, all the magnetic liquid metal exhibited soft magnetic behavior. The magnetic saturation (M_s) of the magnetic liquid metal with Fe/Ni content of 4, 6, 8 and 10 wt% were 11, 12, 13, and 16 emu/g, respectively. Because the liquid metal was non-magnetic, the variation of the M_s must be corresponding for the different contents of the Fe/Ni particles.

Based on the above 3D-printed coaxial microfluidic device and magnetic liquid metal, the monodisperse size controllable MLMDs can be uniformly generated and the sizes are controllable by varying the experimental conditions. Two high accurate syringe pumps (LSP02-1B, Longer-Pump) were used to pump the two phases into the device. The coaxial microfluidic device was connected to syringes through tubes, wherein the inlet for the dispersed phase was directly connected to a syringe to ensure a smooth input of the magnetic liquid metal (Fig. 2d). The droplets were collected in a petri dish with water containing Tween 20 to prevent droplets against spontaneous coalescence. In order to study the controllable range of the droplets diameter, the ratio of the continuous phase (Q_c) and the dispersed phase (Q_d) was changed from 3 to 24 (Q_c/Q_d) because according to Eq. (1) the droplet diameter was a function of the flow rate ratio and the orifice diameter. The orifice diameter of the bottom module was also changed from 250 to 400 μm . As a result, the droplet diameter decreased as the flow rate ratio Q_c/Q_d increased and the orifice diameter became smaller (Fig. 2e). The largest and smallest diameter of the MLMDs was about 650 μm and 1900 μm , respectively. Different orifice diameters corresponded to different droplet diameter variations. The droplet diameter changed from 650 to 1000 μm when the orifice diameter was 250 μm . For the orifice diameter of 300 and 400 μm , the droplets diameter changed from 950 to 1390 μm and 1400 to 1900 μm , respectively. So the droplet diameter could be controlled in the range of 650 to 1900 μm when the flow rate ratio and the orifice diameter of the bottom module were changed. This confirms that the diameter of the generated MLMDs is controllable by changing the experimental conditions (Fang et al. 2019b).

During the preparation, when the orifice diameter was 250 μm , magnetic liquid metal and water containing 15 wt% poly(ethylene glycol)(PEG) were infused at 0.5 mL/h and 12 mL/h, respectively, the average diameter of the as-formed MLMDs was about 650 μm (Fig. 3a). The MLMDs have a uniform diameter distribution with a variation coefficient less than 5% (Fig. S3a), indicating a high reliability of the preparing method. When the infuse speed of the water was decreased from 12 mL/h to 3 mL/h and 2 mL/h, the droplet diameter increased to about 760 and 896 μm (Fig. 3b, c). The variation coefficient of the diameter distribution was all less than 5% (Fig. S3b, c). At the same flow rate ratio, when the orifice diameter was 300 μm and 400 μm , the diameter changed to 971, 1094, 1221 μm (Fig. 3d–f) and 1384, 1518, 1696 μm (Fig. 3g–i). This indicated that the diameter of the monodisperse droplets became larger when the orifice diameter increased. On the other hand, the feasibility of using 3D-printed coaxial microfluidic devices to generate monodisperse size controllable MLMDs was demonstrated. Scanning electron micrograph (SEM) and mapping images

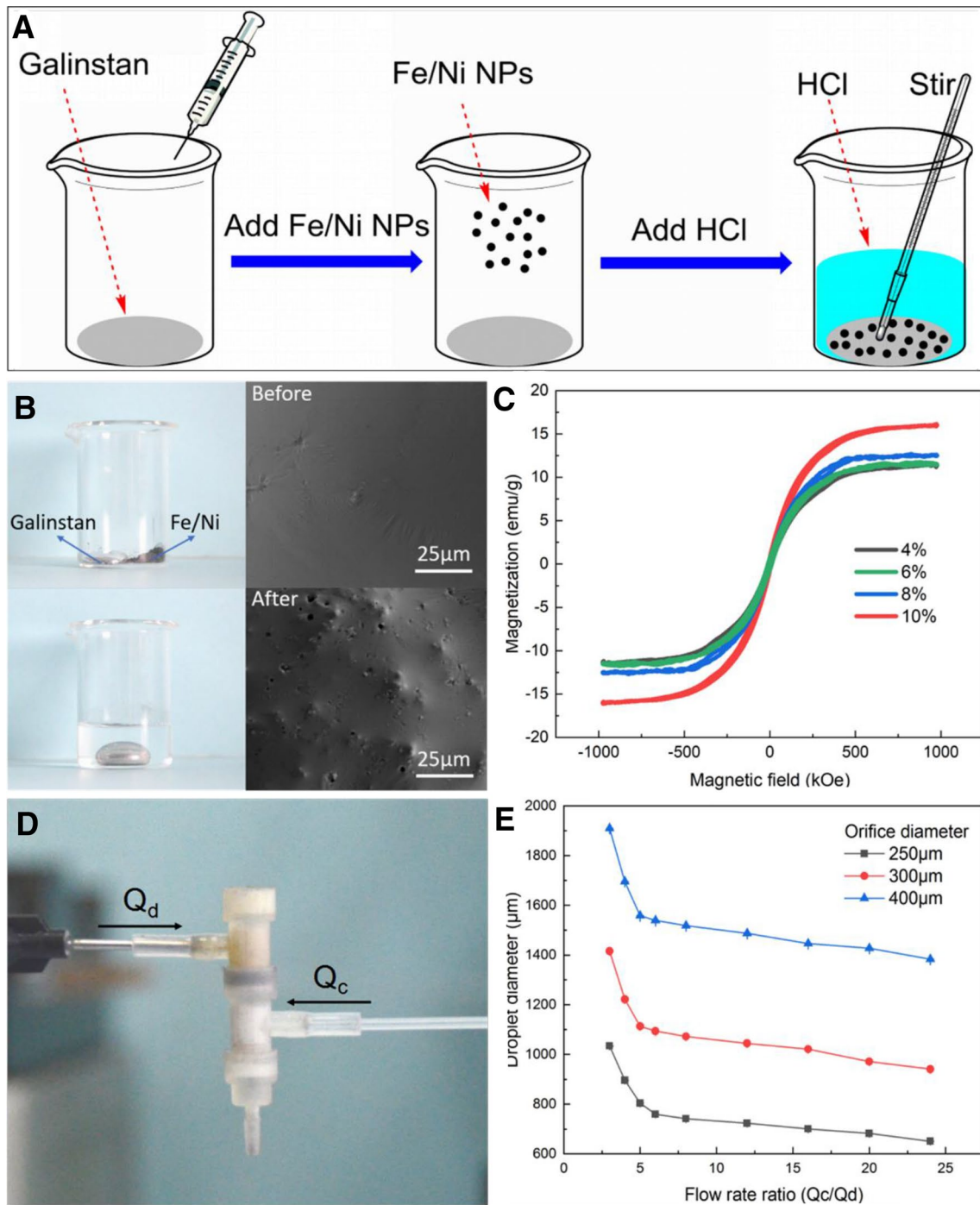


Fig. 2 **a** Schematic diagram of the preparation of magnetic liquid metal. **b** The optical image and SEM image of the liquid metal before and after adding 1 mol/L HCl solution. **c** The magnetic hysteresis loops (magnetization versus an applied magnetic field) of the

MLMDs with different Fe/Ni contents. **d** A macroscopic view of the coaxial microfluidic device used in this study. **e** Relationship between the diameter of the MLMDs and the flow rate ratio of the two phases under different orifice diameters

of the obtained MLMDs (10 wt% Fe/Ni particles) showed that Fe and Ni particles were uniformly distributed in the liquid metal matrix (Fig. 4a). The related energy-dispersive X-ray spectrum (EDX) showed the detailed distribution of the Ga, In, Sn, Fe and Ni elements in the MLMDs (Fig. 4b).

The same results were also found in the MLMDs with 6 wt% and 8 wt% Fe/Ni particles (Fig. S4). The content of Fe/Ni particles was 10 wt% and the relative magnetic force was large enough to make the MLMDs be responsive to the magnetic field. Although the surface of the MLMD was

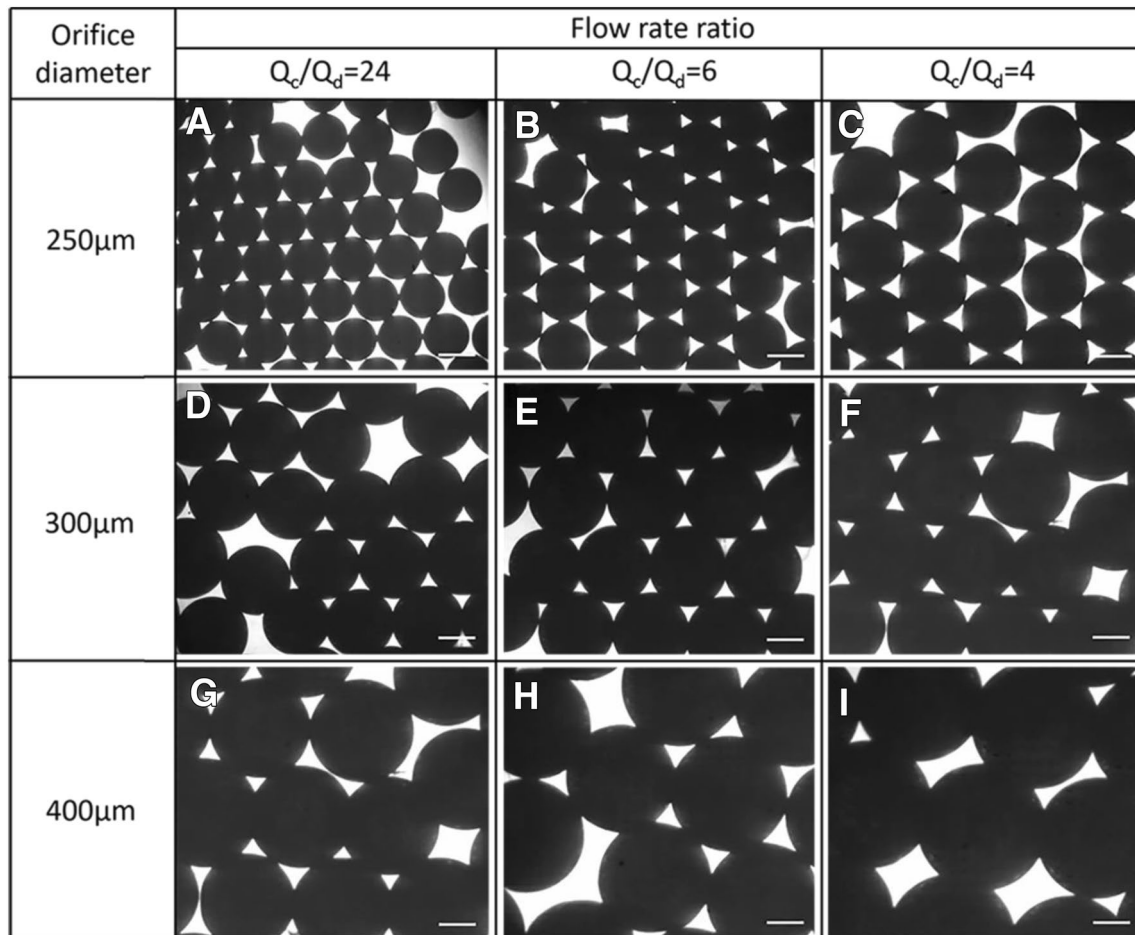


Fig. 3 **a–c** Optical image of the MLMDs using a coaxial microfluidic device at the flow rate ratio of 24, 6 and 4 when the orifice diameter was 250 μm . **d–f** The MLMDs using a coaxial microfluidic device at the flow rate ratio of 24, 6 and 4 when the orifice diameter was

300 μm . **g–i** The MLMDs using a coaxial microfluidic device at the flow rate ratio of 24, 6 and 4 when the orifice diameter was 400 μm . Scale bars: 500 μm

uneven and many protrusions were presented, the liquidity of the MLMDs was well preserved.

3.2 Rheological property of magnetic liquid metal

To control the magnetic manipulation performance, the mass fractions of Fe/Ni particles were varied from 4 wt% to 10 wt%. Here, rheological properties of the magnetic liquid metal under different magnetic flux density were explored by the Anton Paar rheometer (Fig. 5a). Schematic image of the test system was shown in Fig. 5b. The test temperature was 25 $^{\circ}\text{C}$, the shear rate varied from 0.01 to 100 s^{-1} and the maximum magnetic flux density was 720 mT. Figure 5c showed the typical shear rate dependent shear stress of the as prepared magnetic liquid metal. It was found that the shear stress was dependent on the mass fractions of Fe/Ni particles. Obviously, under the same shear rate, the magnetic liquid metal with 10 wt% Fe/Ni content showed higher shear

stress than the others with the mass fractions of 4, 6 and 8 wt%. Figure 5d showed the influence of the shear rate on the viscosity of the magnetic liquid metal with different Fe/Ni contents. It was found that the increased shear rate led the decrement of the viscosity and the viscosity increased with the increase of the Fe/Ni content under a low shear rate ($< 1 \text{ s}^{-1}$). Under the high shear rate, the viscosity of the magnetic liquid metal with different Fe/Ni content tended to be the same, showed a shear thinning behavior.

Figure 5e showed the influence of the magnetic field on the viscosity of the magnetic liquid metal with 10 wt% Fe/Ni content at different shear rate. The viscosities increased with the increase of magnetic field because the increment of the magnetic field caused more internal molecular friction due to the rapid movement of dispersed magnetic particles inside the magnetic liquid metal (Ahmed et al. 2018). The effect of the magnetic field on the viscosity was evident in the case of a small shear rate, but this effect gradually decreased

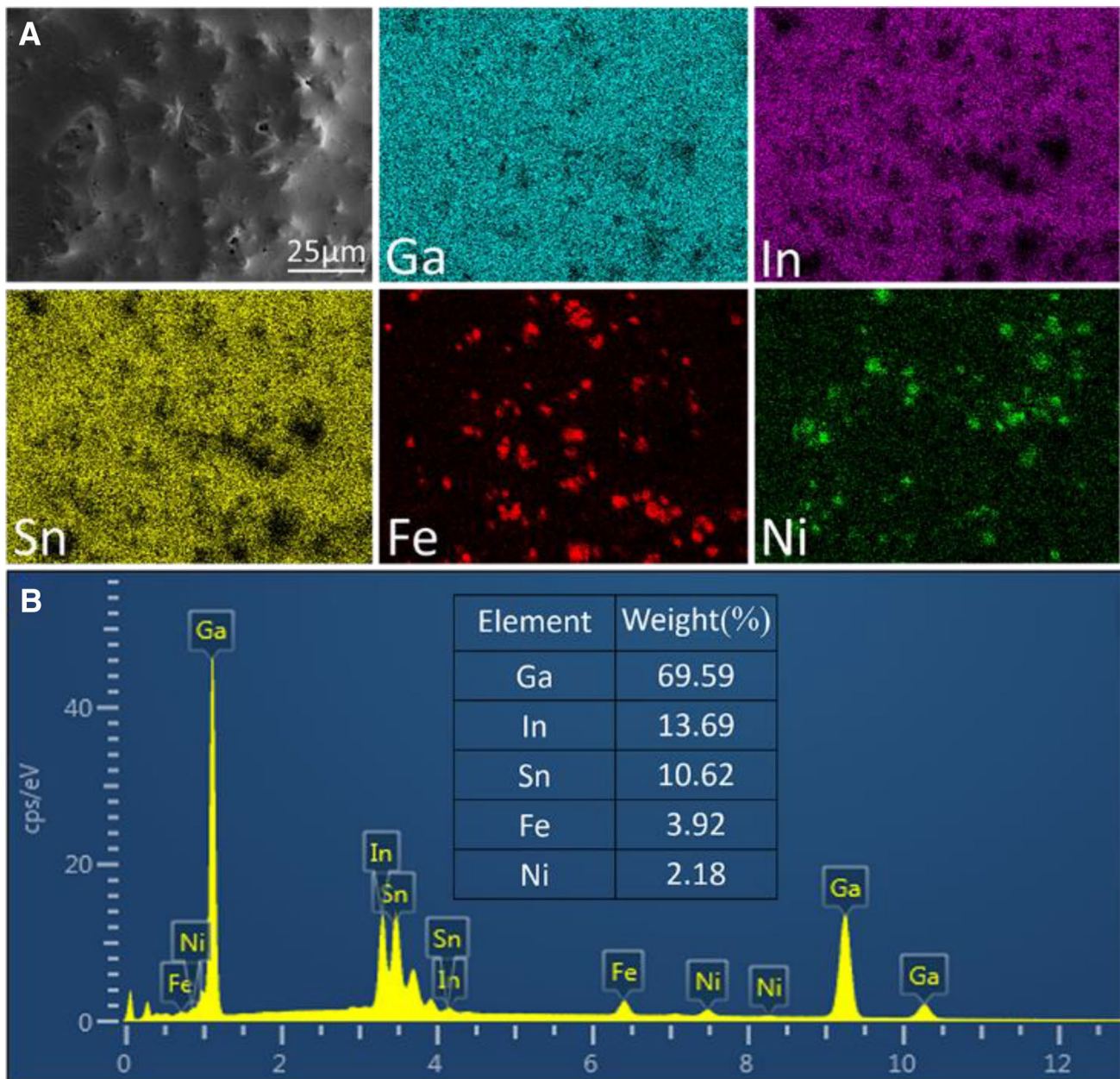


Fig. 4 **a** SEM images of the Fe/Ni particles dispersed in the MLMDs, and the related element mapping of Fe, Ni, Ga, Sn and In, respectively. **b** EDX diagram of the MLMDs and its elemental composition

as the shear rate increased. Figure 5f showed the magnetic field dependent viscosity of the as prepared magnetic liquid metal under the shear rate of 100 s^{-1} . The viscosities of the magnetic liquid metal with different Fe/Ni contents firstly reached the highest value and then tend to level off when the magnetic flux density was above 500 mT. The largest viscosity of the magnetic liquid metal with 10 wt% Fe/Ni content was $5.7\text{ Pa}\cdot\text{s}$, which was higher than the others under the same magnetic field. Similar results were also obtained under the shear rate of 1 s^{-1} and 10 s^{-1} (Fig. S5). This meant that the Fe/Ni content also had a significantly effect on the

viscosity of the magnetic liquid metal (Fang et al. 2019a; Lei et al. 2018; Tong et al. 2018). That is why the increase of magnetic particles content can affect the fluidity of the Galinstan liquid metal.

3.3 Magnetic manipulation of the MLMDs

In order to analyze the magnetic control performance of the MLMDs, the relationship between the diameter of the MLMDs and the minimum magnetic flux density B required to drive the MLMDs with different contents of

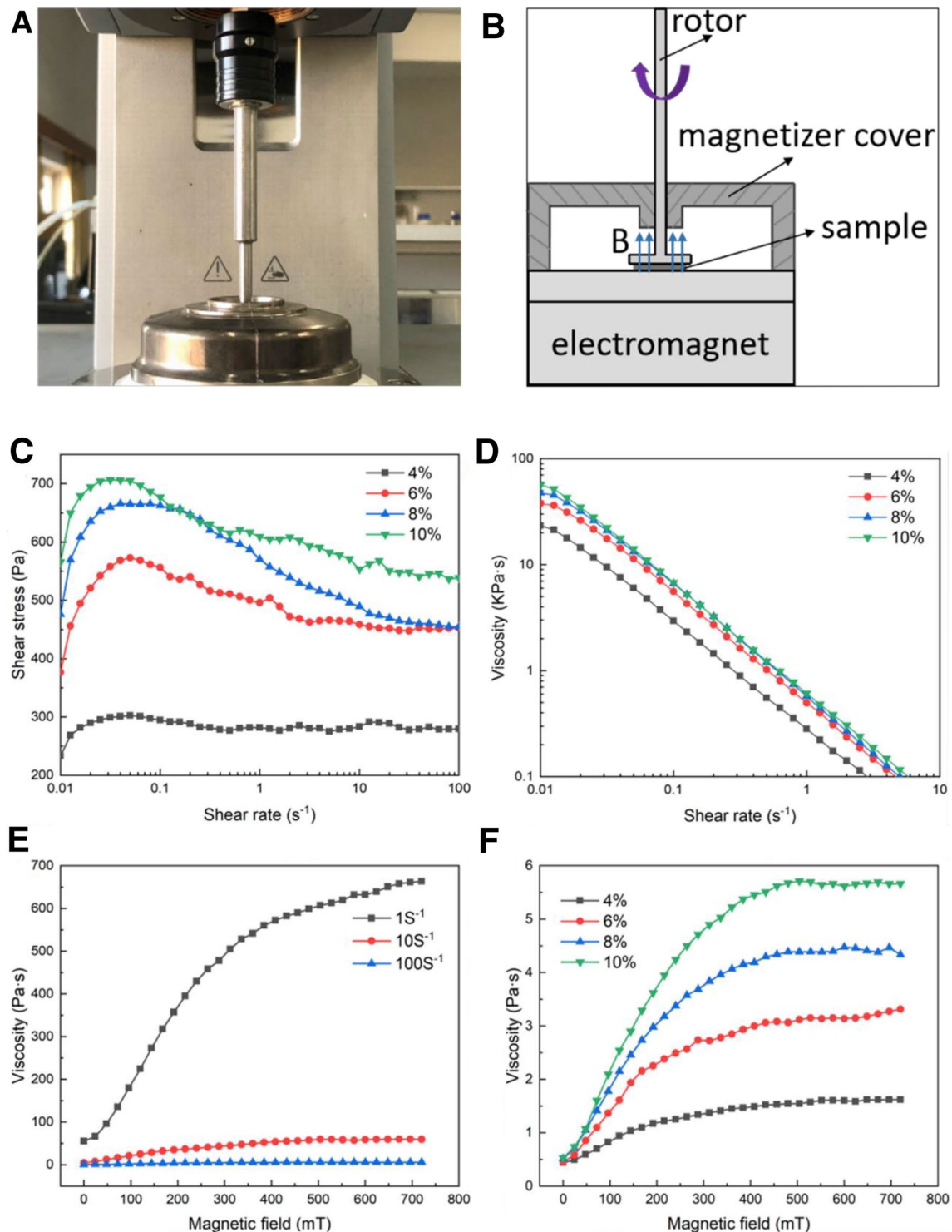


Fig. 5 **a** The photograph of the Anton Paar rheometer. **b** The sketch of the Physica MCR302 test system. **c** Plot of shear stress versus shear rate of the magnetic liquid metal with different Fe/Ni contents. **d** Viscosity versus shear rate of the magnetic liquid metal with differ-

ent Fe/Ni particle contents. **e** Viscosity versus magnetic field of the magnetic liquid metal containing 10 wt% of Fe/Ni particles at different shear rate. **f** Viscosity versus magnetic field of magnetic liquid metal with different Fe/Ni contents at a constant shear rate of 100 s^{-1}

Fe/Ni particles was investigated. Here, the MLMDs with different diameters were sequentially placed in a petri dish filled with 1 mol/L HCl solution. Then a magnet was

placed under the petri dish to slowly approach the MLMD (Fig. 6a), while the probe of a tesla meter was fixed under the MLMD to record the minimum B. Figure 6b showed

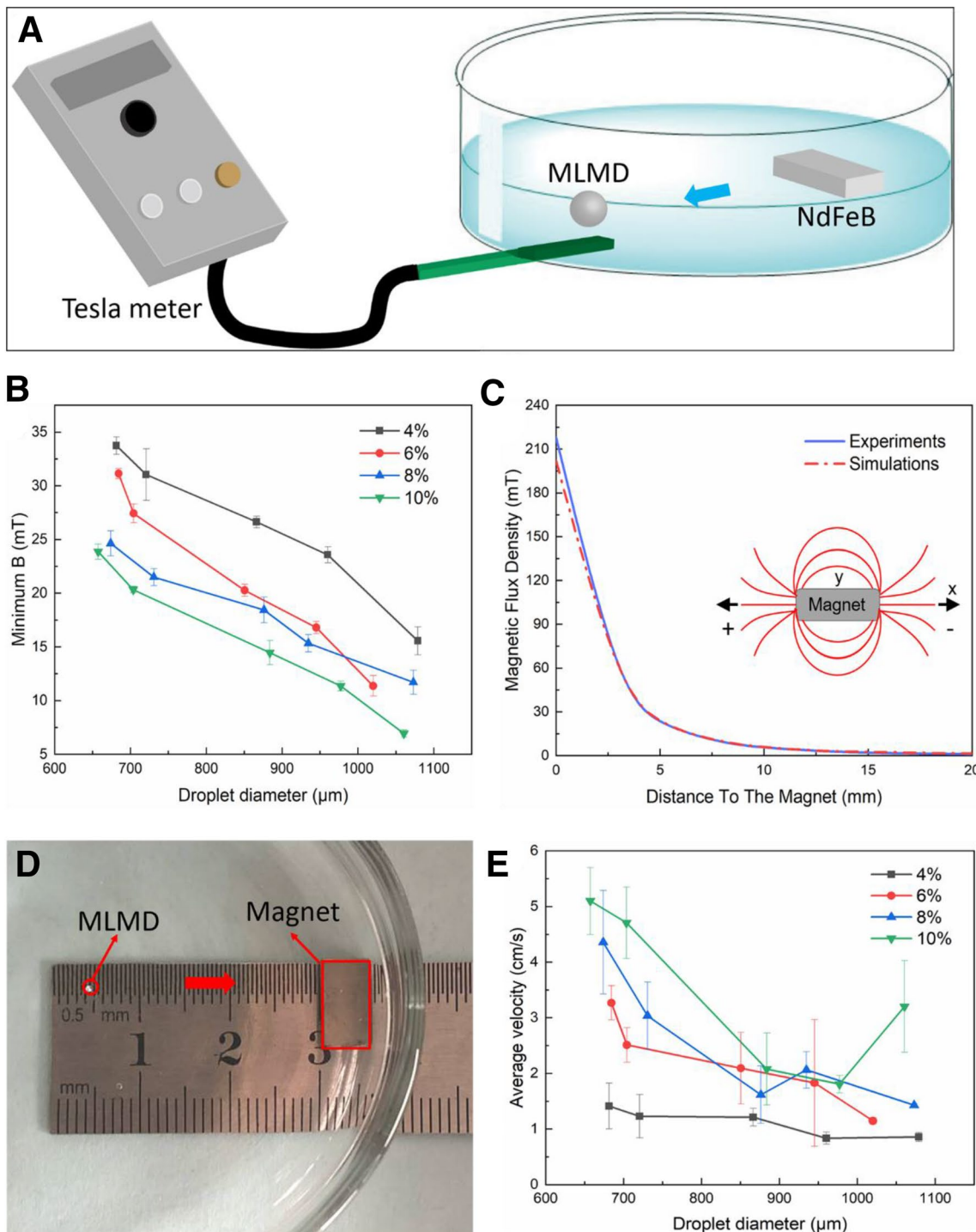


Fig. 6 a Experimental setup for measuring the minimum magnetic flux density **b** Plot of the relationship between the diameter of the MLMDs and the minimum B required to drive the MLMDs with different Fe/Ni contents. **c** Magnetic flux density along the positive direction of x-axis of the magnet. Red dash-dot line for simulations

results. Blue solid line for experimental data measured by a Tesla meter. **d** Experimental setup for measuring the MLMDs' average actuating velocity. **e** Average actuating velocity versus droplet diameter for the MLMDs with different Fe/Ni contents

the relationship between the droplets diameter and the measured minimum B required to drive the MLMDs with different Fe/Ni contents. As the diameter increased, the minimum B required to drive the MLMD gradually decreased under the same Fe/Ni content. The minimum B reduced with the increased content of Fe/Ni particles under the same droplet diameter because the droplets with higher magnetic particle contents had larger magnetism.

Next, the relationship between the average actuating velocity and the diameter of the MLMDs with different Fe/Ni contents under an external magnetic field was also studied. A magnet (NdFeB) was fixed on the steel ruler at the position of 3 cm, which was placed under a petri dish filled with 1 mol/L HCl solution (Fig. 6d). The magnet was slowly brought close to the droplet, and the time required for the droplet to move from the start to the end and the distance elapsed were recorded to calculate the average actuating velocity. Figure 6c presented the value of the magnetic flux density at different distances from the magnet. The maximum value was measured to be 220 mT when the Tesla meter was nearby the magnet and decreased to nearly zero once the distance reached 20 mm. The magnetic flux density was also simulated using COMSOL 4.4 (COMSOL Inc., USA) and the measured values were almost consistent with the results of numerical simulations. Figure S6 showed the numerical simulations of the magnet used in this work. The calculated average actuating velocity of the MLMDs with different diameters was shown in Fig. 6e.

In general, the MLMDs with higher Fe/Ni contents can induce larger actuating velocity under the same diameter. The highest average actuating velocity was 5.10 cm/s for the MLMDs with a high Fe/Ni content of 10 wt%. Under the same content of Fe/Ni particles, the actuating velocity gradually decreased with the diameter increased when the diameter was lower than 900 μm . However, for the MLMDs with higher Fe/Ni contents of 8 wt% and 10 wt%, an increase in velocity could be observed when the diameter was larger than 900 μm . This was because when the droplet moved in HCl solution, it was mainly subjected to the magnetic driving force F_m of the magnet,

$$F_m = 4/3\pi R^3 M \frac{\partial |H_x|}{\partial x} \quad (2)$$

the resistance force F_h in the solution,

$$F_h = \frac{\pi}{2} C \rho_{\text{HCl}} v^2 R^2 \quad (3)$$

and the frictional force f ,

$$f = \frac{4}{3} \pi R^3 \mu g (\rho_{\text{MLM}} - \rho_{\text{HCl}}) \quad (4)$$

here the droplet is assumed to be spherical and the frictional force between the droplet and the substrate is neglected, so the actuating velocity of the droplet can be expressed as,

$$v = \left[\frac{8\pi R^3 h M \frac{\partial |H_x|}{\partial x}}{3(m + \pi R^2 h C \rho_{\text{HCl}})} \right]^{1/2} \quad (5)$$

where M is the magnetization, m and R are the mass and the radius of the droplet, H_x is the magnetic field strength in the x direction, C is the drag coefficient, ρ_{MLM} and ρ_{HCl} denote the density of the droplet and the HCl solution, h is the distance traveled by the droplet and μ is the coefficient of friction. When the diameter is smaller than 900 μm , as the diameter increases, the resistance force F_h grows faster than the magnetic driving force F_m under the same Fe/Ni content, resulting in a gradual decrease in the average actuating velocity. With the increase in Fe/Ni content, the magnetization M increases. Therefore, the growth of magnetic driving force F_m gradually becomes faster according to Eq. (2), and the growth trend becomes more obvious when the diameter becomes larger. So when the diameter is larger than 900 μm , there is an increase in the average actuating velocity for the MLMDs with a Fe/Ni content of 8 wt% and 10 wt%.

3.4 Application of the MLMDs under a magnetic field

Based on the magnetic driven properties of the MLMDs, the magnetic manipulation in a complex channel with different angles was further investigated. A double nozzle high precision 3D printer (Flashforge, Ltd., China) was utilized to print a 1000 μm wide, 800 μm deep channel model with five different angles of 45°, 60°, 90°, 120° and 135° (Fig. 7a). The overall size of the model was 25 mm \times 25 mm \times 2 mm. Figure 7b showed the movement of a MLMD (800 μm , 10 wt% Fe/Ni particles) through the HCl fully-filled channel with different angles (See Movie S1 in the Supporting Information). By placing the magnet under the channel, the MLMD could successfully pass through the turns with different angles. Since the volume of the MLMD was small, separation did not occur when moving at the angle of 90°. This experiment revealed that the MLMD was very flexible and could be manipulated in a limited space using a magnetic field.

The magnetic manipulation of the MLMD (800 μm , 10 wt% Fe/Ni particles) in a three-dimensional spiral channel was also studied. The three-dimensional spiral channel

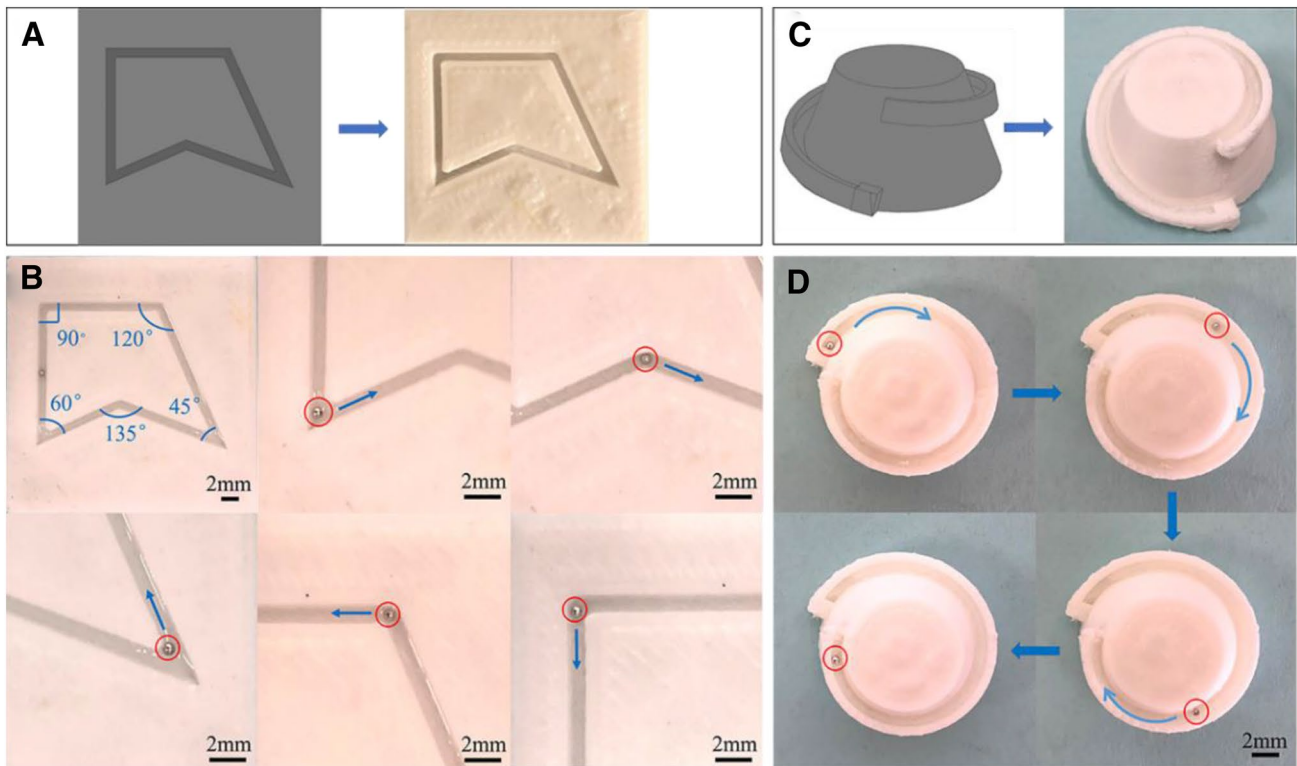


Fig. 7 **a** Schematic diagram of the crooked channel with different angles. **b** Movement of the MLMD in the crooked channel with different angles under a magnetic field. **c** Schematic diagram of the

three-dimensional spiral channel. **d** The MLMD climbs along the three-dimensional spiral channel

model was printed with a top diameter of 12 mm, a bottom diameter of 20 mm and a height of 10 mm (Fig. 7c). The cross-sectional dimension of the channel was 1 mm × 1 mm, and it was filled with HCl solution. Figure 7d showed the entire process of the MLMD climbing from the bottom to the top of the channel (See Movie S2 in the Supporting Information). The MLMD gradually climbed up the channel under the action of a magnet. As the height increased, the friction of the channel wall increased due to the decrease of the HCl solution, which resulted in a decrease of the droplet velocity. However, the whole process could still be completed, confirmed that the droplet had good maneuverability under an external magnetic field.

Based on the above study, the MLMDs can also be applied for electrical switching application due to the electrical conductivity and magnetic field dependent mobility. In this work, an on-off switch model was printed using the 3D printer and the overall size of the model was 35 mm × 10 mm × 2 mm (Fig. 8a). The main channel had a size of 30 mm × 1 mm × 1.2 mm for the movement of a MLMD (800 μm, 10 wt% Fe/Ni particles). The dimensions of the channels located on both sides were 5 mm × 1 mm × 1 mm for embedding the copper wires. The

copper wires were pre-coated with a layer of tin to ensure good contact with the MLMD. The channels located on both sides were slightly higher than the main channel to prevent the wires from contacting with the HCl solution. A 2 mm thick PDMS film was glued to the surface of the switch model and two holes were punched in the film for the ingress and egress of the MLMD.

The MLMD moved with the magnet by positioning the magnet underneath the switch model. When the droplet passed between two wires, the wires were connected and the corresponding LED lights were illuminated (Fig. 8b). By manipulating the MLMD in the channel with the magnetic field, the LEDs were sequentially turned on (See Movie S3 in the Supporting Information). Figure 8c showed the time-lapse images of the magnetic movement of the MLMD in HCl partly-filled main channel. In this experiment, the droplet was successfully manipulated for small-sized electrical switching application, which revealed that the MLMDs exhibited great potential in micro-scale fields. This result also demonstrates that the magnetic manipulation is a promising method for non-contact on-off switch applications.

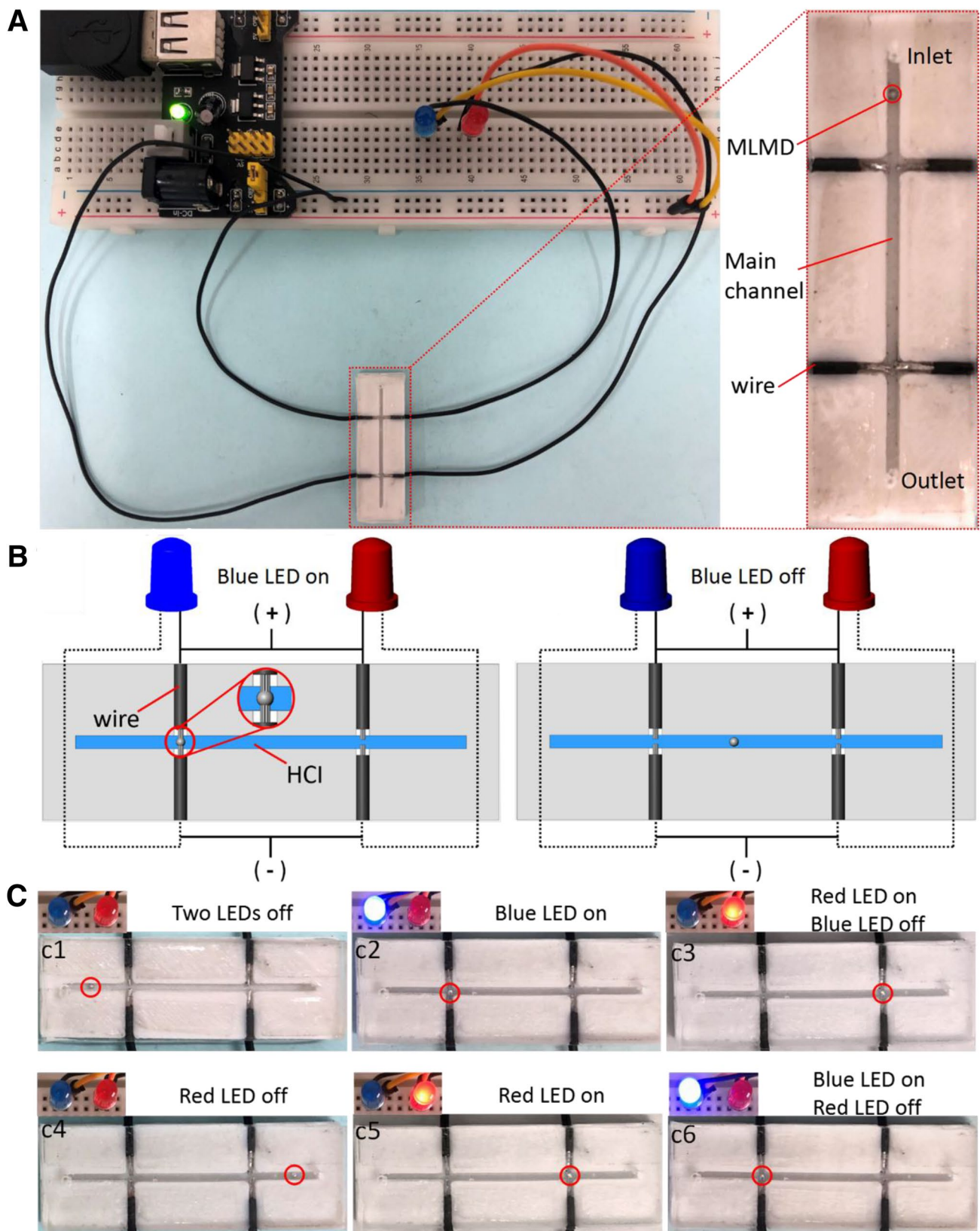


Fig. 8 **a** Schematic diagram of the magnetic control switch model. **b** Conceptual schematic image of manipulating the MLMD to turn on LEDs. **c** Time-lapse images of turning on LEDs by manipulation of the MLMD with an applied magnetic field

4 Conclusion

In this work, an easy method was developed to generate micro-sized MLMDs with controllable size by a 3D-printed coaxial microfluidic device. The MLMDs were composed of Galinstan and Fe/Ni particles, thus it could respond to the magnetic field. Then, the MLMDs with a large diameter variation between 650 and 1900 μm were formed by changing the flow rate ratio of the two phases. Furthermore, the characterization of magnetic properties indicated that a small magnetic flux density can already produce a high actuating velocity when the MLMDs had a high Fe/Ni particle content. The magnetic manipulation of a MLMD was successfully demonstrated in a two-dimensional crooked channel and a three-dimensional spiral channel. Thanks to the high conductivity and magnetic controllability of liquid metal, the small-sized electrical switches based on the MLMDs can be realized. The excellent controllability and good magnetic maneuverability make the MLMDs have wide potential in the micro-scale field, which expands the applicability of liquid metal in diverse practical applications.

Acknowledgements Financial support from the National Natural Science Foundation of China (Grant Nos. 11822209), and the Strategic Priority Research Program of the Chinese Academy of Sciences (Grant No. XDB22040502) are gratefully acknowledged. This study was also supported by the Collaborative Innovation Center of Suzhou Nano Science and Technology, Joint Fund of USTC-National Synchrotron Radiation Laboratory (KY2090000055). Thanks to the instrumentation support from engineering practice center of USTC.

References

- Ahmed A, Qureshi AJ, Fleck BA, Waghmare PR (2018) Effects of magnetic field on the spreading dynamics of an impinging ferrofluid droplet. *J Colloid Interface Sci* 532:309–320
- Bartlett MD, Kazem N, Powell-Palm MJ, Huang XN, Sun WH, Malen JA, Majidi C (2017) High thermal conductivity in soft elastomers with elongated liquid metal inclusions. *Proc Nat Acad Sci USA* 114:2143–2148
- Bhattacharjee N, Urrios A, Kanga S, Folch A (2016) The upcoming 3D-printing revolution in microfluidics. *Lab Chip* 16:1720–1742
- Bilodeau RA, Zemlyanov DY, Kramer RK (2017) Liquid metal switches for environmentally responsive electronics. *Adv Mater Interfaces* 4:1600913
- Chu K, Song BG, Yang HI, Kim DM, Lee CS, Park M, Chung CM (2018) Smart passivation materials with a liquid metal microcapsule as self-healing conductors for sustainable and flexible perovskite solar cells. *Adv Funct Mater* 28:1800110
- Dickey MD (2014) Emerging applications of liquid metals featuring surface oxides. *ACS Appl Mat Inter* 6:18369–18379
- Fang F, Ran SY, Fang ZP, Song PG, Wang H (2019a) Improved flame resistance and thermo-mechanical properties of epoxy resin nanocomposites from functionalized graphene oxide via self-assembly in water. *Composites Part B-Eng* 165:406–416
- Fang QL, Zhang JF, Bai LF, Duan JY, Xu HJ, Leung KCF, Xuan SH (2019b) In situ redox-oxidation polymerization for magnetic core-shell nanostructure with polydopamine-encapsulated-Au hybrid shell. *J Hazard Mater* 367:15–25
- Gu Y, Kojima H, Miki N (2011) Theoretical analysis of 3D emulsion droplet generation by a device using coaxial glass tubes. *Sens Actuators Physic* 169:326–332
- Hu L, Wang HZ, Wang XF, Liu X, Guo JR, Liu J (2019) Magnetic liquid metals manipulated in the three-dimensional free space. *ACS Appl Mat Inter* 11:8685–8692
- Hu T, Xuan SH, Ding L, Gong XL (2018) Stretchable and magneto-sensitive strain sensor based on silver nanowire-polyurethane sponge enhanced magnetorheological elastomer. *Mater Des* 156:528–537
- Hutter T, Bauer WAC, Elliott SR, Huck WTS (2012) Formation of spherical and non-spherical eutectic gallium-indium liquid-metal microdroplets in microfluidic channels at room temperature. *Adv Funct Mater* 22:2624–2631
- Ilyas N, Cook A, Tabor CE (2017) Designing liquid metal interfaces to enable next generation flexible and reconfigurable electronics. *Adv Mater Interfaces* 4:1700141
- Jeon J, Lee JB, Chung SK, Kim D (2016) Magnetic liquid metal marble: characterization of lyophobicity and magnetic manipulation for switching applications. *J Microelectromech Syst* 25:1050–1057
- Jeon J, Lee JB, Chung SK, Kim D (2017) On-demand magnetic manipulation of liquid metal in microfluidic channels for electrical switching applications. *Lab Chip* 17:128–133
- Jeong J, Lee JB, Chung SK, Kim D (2019) Electromagnetic three dimensional liquid metal manipulation. *Lab Chip* 19:3261–3267
- Ji QL, Zhang JM, Liu Y, Li XY, Lv PY, Jin DP, Duan HL (2018) A modular microfluidic device via multimaterial 3D printing for emulsion generation. *Sci Rep* 8:4791
- Jin TM, Hadji EM, Zhao N, Duan ZY, Wang JT (2019) Generation and analysis of axiolitic liquid-metal droplets in a T-Junction microfluidic device. *Chemistryselect* 4:3926–3935
- Khoshmanesh K, Tang SY, Zhu JY, Schaefer S, Mitchell A, Kalantar-Zadeh K, Dickey MD (2017) Liquid metal enabled microfluidics. *Lab Chip* 17:974–993
- Lee CY, Lin YH, Lee GB (2009) A droplet-based microfluidic system capable of droplet formation and manipulation. *Microfluid Nanofluid* 6:599–610
- Lee JM, Zhang M, Yeong WY (2016a) Characterization and evaluation of 3D printed microfluidic chip for cell processing. *Microfluid Nanofluid* 20:5
- Lee S, Kim H, Won DJ, Lee J, Kim J (2016b) On-demand, parallel droplet merging method with non-contact droplet pairing in droplet-based microfluidics. *Microfluid Nanofluid* 20:1
- Lei Q, Zheng C, He F, Zhao J, Liu Y, Zhao XP, Yin JB (2018) Enhancing electroresponsive electrorheological effect and temperature dependence of poly(ionic liquid) particles by hard core confinement. *Langmuir* 34:15827–15838
- Li FX, Kuang SL, Li XP, Shu J, Li WH, Tang SY, Zhang SW (2019) Magnetically- and electrically-controllable functional liquid metal droplets. *Adv Mater Technol* 4:1800694
- Liu TY, Sen P, Kim CJ (2012) Characterization of nontoxic liquid-metal alloy galinstan for applications in microdevices. *J Microelectromech Syst* 21:443–450
- Ma B, Xu CT, Chi JJ, Chen J, Zhao C, Liu H (2019) A versatile approach for direct patterning of liquid metal using magnetic field. *Adv Funct Mater* 29:1901370
- Morimoto Y, Kiyosawa M, Takeuchi S (2018) Three-dimensional printed microfluidic modules for design changeable coaxial microfluidic devices. *Sensors Actuators B-Chem* 274:491–500
- Morimoto Y, Tan WH, Takeuchi S (2009) Three-dimensional axisymmetric flow-focusing device using stereolithography. *Biomed Microdevices* 11:369–377

- Nguyen TH, Chen XM, Sedighi A, Krull UJ, Ren CL (2018) A droplet-based microfluidic platform for rapid immobilization of quantum dots on individual magnetic microbeads. *Microfluid Nanofluid* 22:63
- Shu J, Tang SY, Feng ZH, Li WH, Li XP, Zhang SW (2018) Unconventional locomotion of liquid metal droplets driven by magnetic fields. *Soft Matter* 14:7113–7118
- Song R, Abbasi MS, Lee J (2019) Fabrication of 3D printed modular microfluidic system for generating and manipulating complex emulsion droplets. *Microfluid Nanofluid* 23:92
- Tang SY, Joshipura ID, Lin YL, Kalantar-Zadeh K, Mitchell A, Khoshmanesh K, Dickey MD (2016) Liquid-metal microdroplets formed dynamically with electrical control of size and rate. *Adv Mater* 28:604–609
- Tang SY et al (2014) Liquid metal enabled pump. *Proc Nat Acad Sci USA* 111:3304–3309
- Tong Y, Dong XF, Qi M (2018) Improved tunable range of the field-induced storage modulus by using flower-like particles as the active phase of magnetorheological elastomers. *Soft Matter* 14:3504–3509
- Wang XL, Guo R, Liu J (2019) Liquid metal based soft robotics: materials, designs, and applications. *Adv Mater Technol* 4:1800549
- Wu J, Tang SY, Fang T, Li WH, Li XP, Zhang SW (2018) A wheeled robot driven by a liquid-metal droplet. *Adv Mater* 30:1805039
- Yazdi AA, Popma A, Wong W, Nguyen T, Pan YY, Xu J (2016) 3D printing: an emerging tool for novel microfluidics and lab-on-a-chip applications. *Microfluid Nanofluid* 20:50
- Zhang J, Guo R, Liu J (2016) Self-propelled liquid metal motors steered by a magnetic or electrical field for drug delivery. *J Mater Chem B* 4:5349–5357
- Zhou ZY, Kong TT, Mkaouar H, Salama KN, Zhang JM (2018) A hybrid modular microfluidic device for emulsion generation. *Sensors Actuators Physic* 280:422–428

Publisher's Note Springer Nature remains neutral with regard to jurisdictional claims in published maps and institutional affiliations.